Editors' Suggestion | Featured in Physics

First Observation of Electron Scattering from Online-Produced Radioactive Target

K. Tsukada,[1,2] Y. Abe,[2] A. Enokizono,[2,3] T. Goke,[4] M. Hara,[2] Y. Honda,[2,4] T. Hori,[2] S. Ichikawa,[2,*] Y. Ito,[1] K. Kurita,[3] C. Legris,[4] Y. Maehara,[1] T. Ohnishi,[2] R. Ogawara,[1,2] T. Suda,[2,4] T. Tamae,[4] M. Wakasugi,[1,2] M. Watanabe,[2] and H. Wauke[2,4]

[1]*Institute for Chemical Research, Kyoto University, Uji, Kyoto 611-0011, Japan*
[2]*Nishina Center for Accelerator-Based Science, RIKEN, Wako, Saitama 351-0198, Japan*
[3]*Department of Physics, Rikkyo University, Toshima, Tokyo 171-8501, Japan*
[4]*Research Center for Electron Photon Science, Tohoku University, Sendai, Miyagi 982-0826, Japan*

(Received 7 March 2023; accepted 21 June 2023; published 30 August 2023)

We successfully performed electron scattering off unstable nuclei which were produced online from the photofission of uranium. The target ^{137}Cs ions were trapped with a new target-forming technique that makes a high-density stationary target from a small number of ions by confining them in an electron storage ring. After developments of target generation and transportation systems and the beam stacking method to increase the ion beam intensity up to approximately 2×10^7 ions per pulse beam, an average luminosity of 0.9×10^{26} cm^{-2} s^{-1} was achieved for ^{137}Cs. The obtained angular distribution of elastically scattered electrons is consistent with a calculation. This success marks the realization of the anticipated femtoscope which clarifies the structures of exotic and short-lived unstable nuclei.

DOI: 10.1103/PhysRevLett.131.092502

Short-lived unstable nuclei have been intensively investigated worldwide following the discovery of exotic phenomena, such as halos, neutron skins, and losses and appearances of nuclear magicities [1]. Advances in accelerator technology and the radioactive isotope (RI) production method have helped expand the accessible areas of unstable nuclei in the nuclear chart and improved the understanding of those exotic features of interest not only for the study of nuclear structures, but also for applications such as nucleosynthesis in the field of astrophysics [2]. The sizes and shapes of nuclei are particularly important for establishing nuclear structure models that can be applied to these unstable nuclei. The root-mean-squared (rms) nuclear-matter (both proton and neutron) radii of unstable nuclei have been measured using the total reaction cross section with a transmission method [3]. Elastic proton scattering in inverse kinematics with an RI beam provides nuclear-matter distribution information [4,5]. These methods use hadronic probes to investigate unstable nuclei owing to their relatively large reaction rates, but they are affected by unavoidable ambiguities in the reaction mechanism due to the strong nuclear force.

Electron scattering is one of the most powerful and reliable tools for investigating the internal structure of atomic nuclei owing to its weakness compared to the strong nuclear force and its well-understood interaction mechanism [6]. Many important features of atomic nuclei have been unambiguously clarified via high-energy electron scattering aimed at stable nuclei since Hofstadter and his colleagues established the effectiveness of electron scattering for nuclear structure studies approximately a half century ago [7]. The spatial charge density distribution in the nucleus is an important feature determined by elastic electron scattering, because it is directly related to the sum of squares of all proton wave functions in the independent single-particle model. The rms charge radii of nuclei including unstable ones have been determined by isotope shift measurements via laser spectroscopies [8,9], which are very precise but sensitive to only the relative radius difference between two isotopes. The investigation of unstable nuclei via elastic electron scattering provides important and direct information for understanding their internal structures, as it clearly determines not only the size, but also the shape by measuring the diffraction pattern of the charge form factors. However, electron scattering has not been applied to unstable nuclei thus far. A few exceptions are, for example, ^{3}H, ^{14}C, and ^{41}Ca, whose lifetimes of 12.3, 5700, and 10^5 yr, respectively, are long enough to prepare targets of adequate thickness [10–12]. For example, a 1-g ^{3}H target was used to achieve the luminosity required for electron scattering experiments [13]. It is, however, impossible to prepare a large amount of targets for more production-hard, short-lived unstable nuclei. To overcome this difficulty and realize electron scattering for short-lived unstable nuclei, we developed a novel internal target-forming technique, self-confining RI ion target (SCRIT) [14]. It allows us to form a stationary target along the electron beam and achieve high luminosity with a small number of online-produced radioactive nuclear ions owing to the effective large current in a storage ring. The target ions are prepared at an isotope separation online (ISOL) system and transported to the SCRIT system [15]

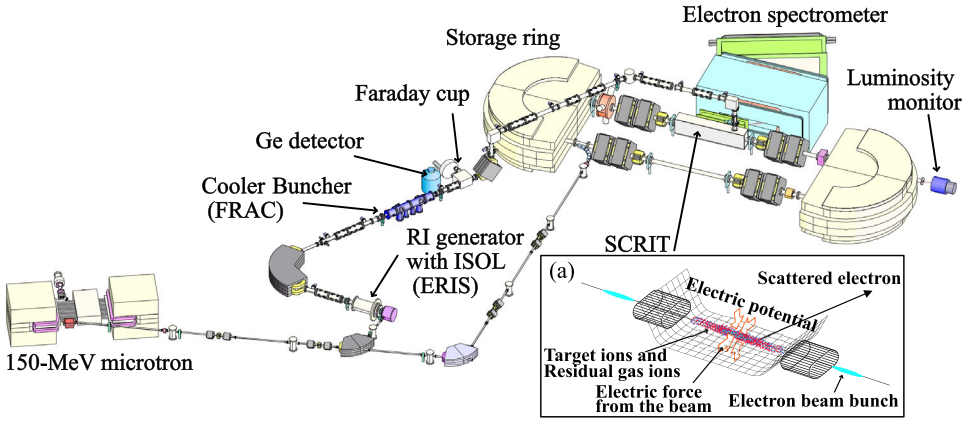

FIG. 1. Floor plan of the SCRIT electron scattering facility. The facility consists of a 150-MeV microtron, an electron storage ring equipped with the SCRIT system, an RI generator with ISOL and transportation system, a scattered electron spectrometer, and a luminosity monitor. (a) shows the conceptual design of the SCRIT method.

before they decay within their lifetime. After we successfully confirmed the principle of the SCRIT method experimentally [16], we started building an electron scattering facility [17] based on the SCRIT technique in the RIKEN RI beam factory [18] building in 2009, which has been completed in recent years [19]. In this Letter, we report the world's first elastic electron scattering results obtained from an online-produced radioactive nuclear target.

Figure 1 shows a schematic view of the SCRIT facility that consists of an electron storage ring equipped with the SCRIT device, ISOL system, cooler buncher in the ion transportation system, 150-MeV electron microtron used as the electron injector and the ISOL driver, an electron spectrometer, and a luminosity monitor. Figure 1(a) shows the concept of the SCRIT method. The SCRIT device consists of three electrodes aligned along the electron beam, which cylindrically surround the electron beam. The two end electrodes form an electrostatic potential barrier as shown in Fig. 1(a), while the third electrode surrounds the whole region: the trapping region and the end electrodes. The electric potential of the trapping region was slightly lower than 6 kV, the kinetic energy of the injected target ions, and the barrier potentials were 6.6 kV. Therefore, the target ions were trapped with the kinetic energy of less than a few eV. It has been confirmed using stable nuclear ions that a luminosity of 10^{27} $\mathrm{cm}^{-2}\,\mathrm{s}^{-1}$ was achieved with an effective target thickness of 10^{9} cm^{-2} and an average electron beam current of 200 mA by introducing only 10^{8} particles into the SCRIT system [19]. This luminosity is required to determine the charge density distribution of medium-heavy nuclei.

Recently, we successfully performed elastic electron scattering from an online-produced radioactive nuclear target, ^{137}Cs, for the first time. ^{137}Cs has a lifetime of 30 yr, which is not short, but this experiment perfectly mimics a short-lived unstable nucleus, as shown below. An electron beam with an energy of 149.3 MeV was stored in the storage ring. The stored beam current was approximately 200 mA on average. After beam injection into the storage ring, uranium carbides comprised of 28-g uranium were irradiated with a 15-W electron beam to produce radioactive nuclides via the photofission process. The generated cesium nuclides were ionized using the surface ionization technique in the ISOL system [15], and the ion beams prepulsed by a grid action in the ion source were extracted at a frequency of 40 Hz. ^{137}Cs was selected as the target because of its high extraction and transportation efficiencies resulting from the surface ionizing technique with low ionization energy. The cooler buncher, a fringing-rf-field-activated dc-to-pulse converter (FRAC) [20], accepted the prepulsed ^{137}Cs ion beam with little or no loss; the FRAC stacked the beam for 4 s by repeating the injection and cooling by colliding with a pressure-controlled neon buffer gas at 2×10^{-3} Pa and then ejected it as a pulsed beam at a frequency of 0.25 Hz. The obtained extraction rates of cesium and barium isotopes for the electron-beam-driven RI separator for SCRIT (ERIS) are shown in Fig. 2. ALTO data [21] are also shown as a reference. The barium isotope ions were considered the main contaminants of the cesium ion beam, because they were similarly generated via the uranium photofission process and ionized in the same manner. Furthermore, they were continuously supplied by the beta decay of cesium nuclei. Production rates of other nuclides were very small because of the relatively low temperature of the ionization chamber, about 1200 °C. Relative amounts of cesium isotopes were measured with a Faraday cup, and the absolute amount was calibrated by ^{140}Cs amount obtained from gamma decay rates measured with a Ge detector. The Faraday cup and Ge detector were placed behind the FRAC, as shown in Fig. 1. ALTO data are also normalized for ^{140}Cs. The amount of ^{137}Ba contamination in the ^{137}Cs beam was evaluated by measuring the amount of ^{139}Ba with the Ge detector, because the lifetime of ^{137}Cs is too long to directly measure the amounts of ^{137}Cs and ^{137}Ba. At our

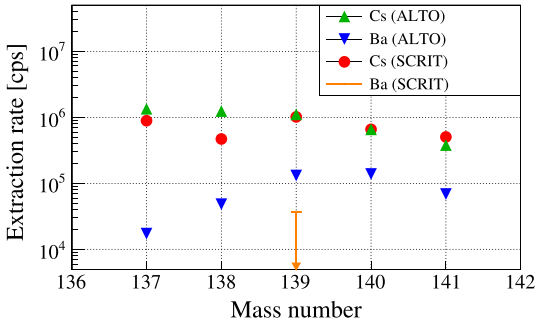

FIG. 2. Achieved extraction rates of the cesium and barium isotopes. ALTO data [21] are also drawn as a reference. The mass number dependence among cesium isotopes was measured using a Faraday cup, and the absolute value was determined by measuring the gamma ray from ^{140}Cs. The ALTO data are normalized to the amount of ^{140}Cs at the SCRIT. The amount of ^{137}Ba contamination in the ^{137}Cs beam was calculated to be less than 0.5% from the amount of ^{139}Ba, which is low, and only the upper end of the error bar is shown.

facility, the amount of ^{139}Ba was obtained to be very low and is shown with only the upper end of the error bar in Fig. 2. Statistical errors for cesium isotopes are smaller than the symbol size. Although the ratio between cesium and barium ions can vary due to different experimental conditions between the two facilities, the isotope dependences can be safely assumed to be similar. Cesium isotopes were supplied not only by the direct photofission process, but also from the weak decay of xenon isotopes generated by the photofission process. In Fig. 2, the amounts of ^{137}Cs and ^{138}Cs seem to be smaller than those of ALTO data. This is because the measurement time of isotope dependence was short to reach the equilibrium state compared to the lifetimes of ^{137}Xe and ^{138}Xe. The purity of the ^{137}Cs beam was evaluated to be more than 99.5%.

Approximately 10^7 ^{137}Cs ions per pulse were delivered into the SCRIT with 1.9 s trapping and then released to maintain the target quality, considering the escape of highly charged target ions and the increase of trapped residual gas ions. As they entered highly charged states, trapped ions, both target ions and residual gas ions, became attracted to the beam center by the electric force from the beam bunch and escaped from the trapping region due to beam instabilities. The injection-trapping-release cycle was repeated at a frequency of 0.5 Hz. To evaluate the background contribution with a null target condition, ^{137}Cs ions were injected every two cycles. The scattered electrons were detected using the spectrometer consisting of a large-aperture dipole magnet and two drift chambers in front of and behind the magnet to reconstruct the trajectories of scattered electrons. The spectrometer covers a scattering angle of 30°–60°, with a total solid angle of approximately 80 msr. The momentum resolution was $\delta p/p = 3 \times 10^{-3}$ for scattered electrons of 150 MeV. The luminosity was continuously monitored by counting the bremsstrahlung photons with CsI calorimeters located 7 m downstream from the SCRIT device. The average luminosity of this experiment was evaluated to be 0.9×10^{26} cm^{-2} s^{-1} and almost constant within the 1.9 s trapping time. The statistical error of the luminosity is less than 2%, and the systematic error on the luminosity determination is less than 10%.

Figure 3 shows reconstructed reaction vertex distributions along the beam (Vz) and the vertical direction (Vy)

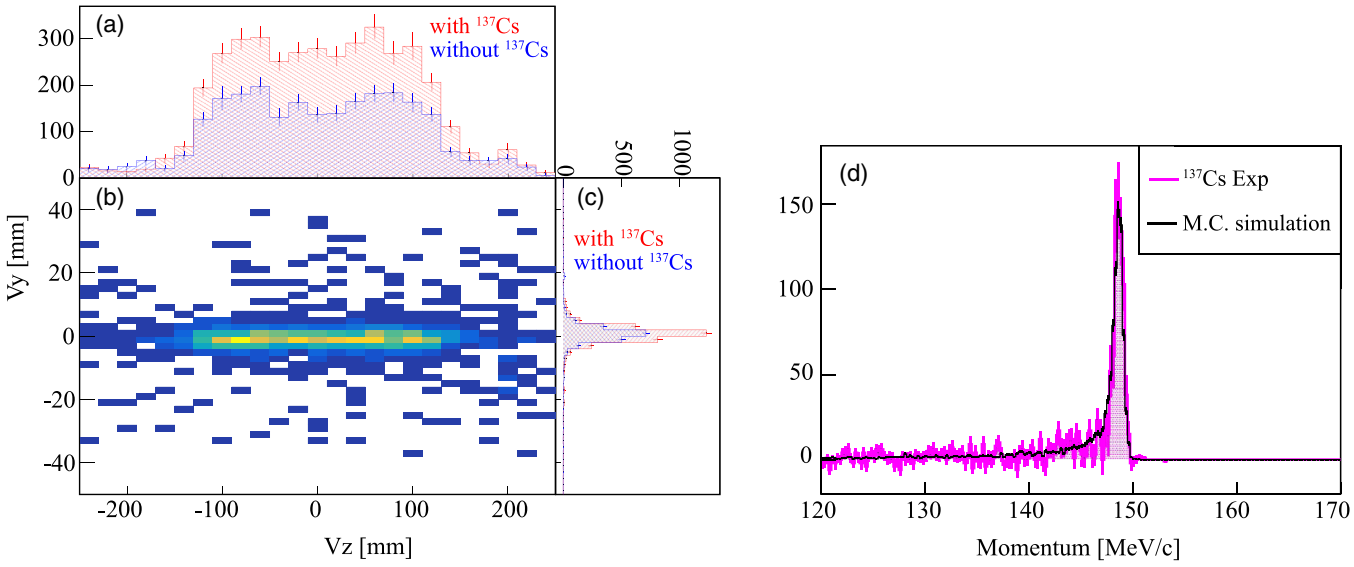

FIG. 3. Reconstructed reaction vertex and momentum distributions. (a) and (c) show the vertex distributions along the beam and vertical directions with and without ^{137}Cs ions (red and blue histograms, respectively). (b) shows the two-dimensional vertex distribution with ^{137}Cs ions. (d) shows the momentum distribution after background subtraction. The black histogram is a Monte Carlo simulation based on the GEANT4 toolkit [22].

and the momentum distribution of scattered electrons coming from the target region. Figure 3(b) shows the correlation between Vy and Vz, and Figs. 3(a) and 3(c) are the one-dimensional projections with and without ^{137}Cs for elastic scattering events, respectively. The vertex resolutions are evaluated to be 3 and 2 mm in σ for Vz and Vy, respectively. Elastic scattering events observed without ^{137}Cs are attributable to residual gases consisting primarily of oxygen and carbon, which are the main background sources. As shown in Figs. 3(a) and 3(c), both ^{137}Cs and residual gas ions were uniformly trapped along the electron beam. The signal-to-noise ratio is approximately 1, because the achieved luminosity of ^{137}Cs was still one order of magnitude lower than the designed value. The contribution of backgrounds was safely subtracted in the subsequent analysis, because the amount of residual gas ions was little affected by the small amount of ^{137}Cs ions. The ambiguity of the background evaluation is approximately 10% at the present, which causes the largest systematic error associated with the angular dependence of the cross sections. This error will be reduced by studying the behavior of the ions trapped in the SCRIT and improving the signal-to-noise ratio. The effective target length of approximately 250 mm is shorter than the geometrical length of the 500-mm-long SCRIT electrodes due to the tails of the barrier potentials. Figure 3(d) shows a reconstructed momentum spectrum after background subtraction. An elastic peak is clearly observed. The black histogram is a result of Monte Carlo simulation based on the GEANT4 toolkit [22], which reproduces our spectrum well, including the radiation tail. Figure 4 shows the angular dependence of elastic scattering for both ^{137}Cs and the residual gas background. The angular resolution at the target is evaluated to be 0.5° by the simulation, mainly due to multiple scattering effects in the 2-mm-thick beryllium window. Corrections for spectrometer acceptance evaluated by the simulation were applied. The error bars represent the statistical error only. The vertical axis denotes $Ld\sigma/d\Omega$ $(\mathrm{cm}^{-2}\,\mathrm{s}^{-1})(\mathrm{cm}^2/\mathrm{sr})$, where L and $d\sigma/d\Omega$ are the luminosity and the differential cross section, respectively. The slope of ^{137}Cs is noticeably steeper than that of the residual gas, which represents the radius difference between ^{137}Cs and the residual gas. The scattering angle region from 30° to 56° at an electron beam energy of 149 MeV corresponds to momentum transfer from 0.4 to 0.7 fm^{-1}. In this low-momentum transfer region, the cross section is dominated by the electric monopole component of the elastic scattering process even though ^{137}Cs has a spin parity of $I^P = 7/2^+$ in its ground state. The contributions from higher multipoles, such as the electric quadrupole and magnetic dipole in elastic processes and nuclear excited states in inelastic processes, are negligible compared with the statistical error of the present data. Two lines are derived from calculations using DREPHA [23], which is a phase shift calculation code to calculate the cross section of elastic electron scattering from a spherical nucleus. A two-parameter Fermi distribution, $\rho(r) = \rho_0/[1 + \exp 4\ln 3(r-c)/t]$, is assumed as the charge density distribution of ^{137}Cs, where ρ_0 is the normalization factor and c and t are the radius and surface distribution parameters, respectively. The two parameters are fixed at $c = 5.683$ fm and $t = 2.3$ fm to reproduce the rms radius of 4.813 fm determined by the isotope shift experiment [8]. The charge density distribution of the ^{16}O nucleus [24] is considered the main component for calculating the residual gas background. The measured angular dependencies are found to be well reproduced by these theoretical calculations.

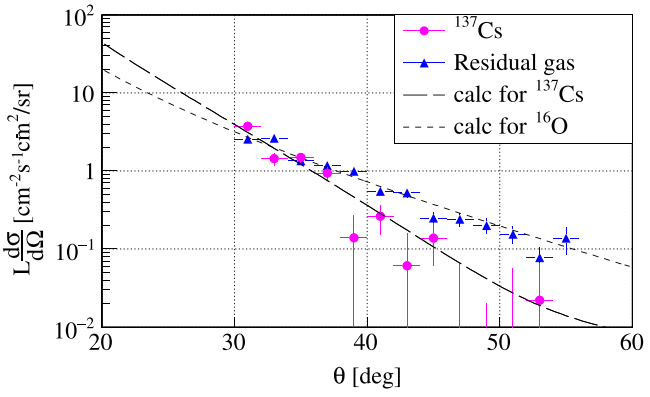

FIG. 4. Obtained angular distribution for ^{137}Cs and residual gas. Different slopes of the angular dependences for ^{137}Cs and residual gas imply the radius difference of the target nuclei. Two lines are derived from calculations using the DREPHA code [23], assuming the two-parameter Fermi distribution for the nuclear charge density distributions.

This is clear evidence of the successful demonstration of electron scattering experiments targeting online-produced radioactive nuclei. Although the obtained luminosity of 0.9×10^{26} $\mathrm{cm}^{-2}\,\mathrm{s}^{-1}$ is still lower than the design value of 10^{27} $\mathrm{cm}^{-2}\,\mathrm{s}^{-1}$ required for determining the charge density distribution of medium-heavy nuclei, a luminosity improvement can be accomplished by simply increasing the power of the ISOL driver from 15 W to 2 kW at the next facility upgrade within a few years. After upgrading, the signal-to-noise ratio will be greatly improved, and the charge density distribution of various short-lived unstable nuclei, such as ^{132}Sn and its isotopes, will be investigated by electron scattering.

In conclusion, we observed for the first time elastically scattered electrons from ^{137}Cs nuclei that were produced by the photofission of uranium. This result indicates the establishment of the SCRIT scheme to realize electron scattering from online-produced radioactive nuclei and paves the way for electron scattering studies of short-lived unstable nuclei. This is a long-awaited method, as the femtoscope, that reveals the structure of short-lived

unstable nuclei with unambiguous and well-calculable electromagnetic interaction.

This work was supported by JSPS KAKENHI Grants No. JP22224004, No. JP17H04835, and No. JP20H00147.

[*]Deceased.

[1] T. Nakamura, H. Sakurai, and H. Watanabe, Exotic nuclei explored at in-flight separators, Prog. Part. Nucl. Phys. **97**, 53 (2017).

[2] T. Kajino, W. Aoki, A. B. Balantekin, R. Diehl, M. A. Famiano, and G. J. Mathews, Current status of r-process nucleosynthesis, Prog. Part. Nucl. Phys. **107**, 109 (2019).

[3] A. Ozawa, Matter radii and density distributions, in *Handbook of Nuclear Physics*, edited by I. Tanihata, H. Toki, and T. Kajino (Springer, Singapore, 2022), 10.1007/978-981-15-8818-1_40-1.

[4] M. von Schmid, S. Bagchi, S. Bnig, M. Csatls. I. Dillmann, C. Dimopoulou, P. Egelhof, V. Eremin, T. Furuno, H. Geissel *et al.* (EXL Collaboration), Investigation of the nuclear matter distribution of ^{56}Ni by elastic proton scattering in inverse kinematics, Phys. Scr. **2015**, 014005 (2015).

[5] H. Sakaguchi and J. Zenihiro, Proton elastic scattering from stable and unstable nuclei—Extraction of nuclear densities, Prog. Part. Nucl. Phys. **97**, 1 (2017).

[6] T. Suda and H. Simon, Prospects for electron scattering on unstable, exotic nuclei, Prog. Part. Nucl. Phys. **96**, 1 (2017).

[7] B. Hahn, D. G. Ravenhall, and R. Hofstadter, High-energy electron scattering and the charge distributions of selected nuclei, Phys. Rev. **101**, 1131 (1956).

[8] I. Angeli, A consistent set of nuclear rms charge radii: Properties of the radius surface R(N,Z), At. Data Nucl. Data Tables **87**, 185 (2004).

[9] P. Campbell, I. D. Moore, and M. R. Pearson, Laser spectroscopy for nuclear structure physics, Prog. Part. Nucl. Phys. **86**, 127 (2016).

[10] I. Sick, Elastic electron scattering from light nuclei, Prog. Part. Nucl. Phys. **47**, 245 (2001).

[11] F. J. Kline, H. Crannell, J. T. O'Brien, J. McCarthy, and R. R. Whitney, Elastic electron scatterring from ^{14}C, Nucl. Phys. **A209**, 381 (1973).

[12] H. Baghaei, A. Cichocki, J. B. Flanz, M. Frodyma, B. Frois, Y. Han, R. S. Hicks, J. Martino, R. A. Miskimen, C. N. Papanicolas *et al.*, Elastic magnetic electron scattering from ^{41}Ca, Phys. Rev. C **42**, 2358 (1990).

[13] F. P. Juster, S. Auffret, J. M. Cavedon, J. C. Clemens, B. Frois, D. Goutte, M. Huet, P. Leconte, J. Martino, Y. Mizuno *et al.*, Tritium Electromagnetic Form Factors, Phys. Rev. Lett. **55**, 2261 (1985).

[14] M. Wakasugi, T. Emoto, Y. Fukukawa, K. Ishii, S. Ito, T. Koseki, K. Kurita, A. Kuwajima, T. Matsuda, A. Morikawa *et al.*, Novel Internal Target for Electron Scattering off Unstable Nuclei, Phys. Rev. Lett. **100**, 164801 (2008).

[15] T. Ohnishi, S. Ichikawa, K. Koizumi, K. Kurita, Y. Miyashita, R. Ogawara, S. Tamaki, M. Togasaki, and M. Wakasugi, Electron-beam-driven RI separator for SCRIT (ERIS) at RIKEN RI beam factory, Nucl. Instrum. Methods Phys. Res., Sect. B **317**, 357 (2013).

[16] T. Suda, M. Wakasugi, T. Emoto, K. Ishii, S. Ito, K. Kurita, A. Kuwajima, A. Noda, T. Shirai, T. Tamae *et al.*, First Demonstration of Electron Scattering Using a Novel Target Developed for Short-Lived Nuclei, Phys. Rev. Lett. **102**, 102501 (2009).

[17] M. Wakasugi, T. Ohnishi, S. Wang, Y. Miyashita, T. Adachi, T. Amagai, A. Enokizono, A. Enomoto, Y. Haraguchi, M. Hara *et al.*, Construction of the SCRIT electron scattering facility at the RIKEN RI Beam Factory, Nucl. Instrum. Methods Phys. Res., Sect. B **317**, 668 (2013).

[18] Y. Yano, The RIKEN RI beam factory project: A status report, Nucl. Instrum. Methods Phys. Res., Sect. B **261**, 1009 (2007).

[19] K. Tsukada, A. Enokizono, T. Ohnishi, K. Adachi, T. Fujita, M. Hara, M. Hori, T. Hori, S. Ichikawa, K. Kurita *et al.*, First Elastic Electron Scattering from ^{132}Xe at the SCRIT Facility, Phys. Rev. Lett. **118**, 262501 (2017).

[20] M. Wakasugi, M. Togasaki, T. Ohnishi, K. Kurita, R. Toba, M. Watanabe, and K. Yamada, FRAC: Fringing-RF-field-activated dc-to-pulse converter for low-energy ion beams, Rev. Sci. Instrum. **89**, 095107 (2018).

[21] S. Essabaa, N. Boscher, M. C. Mhamed, E. Cottereau, S. Franchoo, F. Ibrahim, C. Lau, B. Roussire, A. Sad, S. Tusseau-Nenez *et al.*, The radioactive beam facility ALTO, Nucl. Instrum. Methods Phys. Res., Sect. B **317**, 218 (2013).

[22] S. Agostinelli *et al.*, GEANT4—A simulation toolkit, Nucl. Instrum. Methods Phys. Res., Sect. A **506**, 250 (2003).

[23] B. Dreher, A phase-shift calculation code for elastic electron scattering, communicated by J. Friedrich.

[24] H. de Vries, C. W. de Jager, and C. de Vries, Nuclear charge-density-distribution parameters from elastic electron scattering, At. Data Nucl. Data Tables **36**, 495 (1987).